Collisions of slow electrons with SiF_4 and GeF_4: Shape resonance, Ramsauer-Townsend minimum, and virtual state

G. M. Moreira and M. H. F. Bettega
Departamento de Física, Universidade Federal do Paraná, Caixa Postal 19044, 81531-990 Curitiba, Paraná, Brazil
(Received 29 February 2016; published 7 June 2016)

We report calculated elastic integral, differential, and momentum transfer cross sections for electron impact with the tetrahalides SiF_4 and GeF_4. The cross sections were computed with the Schwinger multichannel method with pseudopotentials in the static-exchange and static-exchange plus polarization approximations and for energies up to 12 eV. Our results are compared with theoretical and experimental results available in the literature, and in general the agreement is quite good. In addition, we report the presence of a Ramsauer-Townsend minimum and of a T_2 shape resonance in the integral cross section of SiF_4, and the presence of a virtual state and also of a T_2 shape resonance in the GeF_4 cross section. These features were also observed and discussed by some experiments and calculations.

DOI: 10.1103/PhysRevA.93.062702

I. INTRODUCTION

Silicon and germanium tetrahalides (SiF_4 and GeF_4, respectively) are molecules widely used as feed gases in plasma processes (mainly in semiconductor fabrication), such as ion implantation, etching, and chemical vapor deposition. The modeling and simulation of plasma reactors requires several inputs regarding the feed gas to be used in these plasma processes [1,2], such as the various types of cross sections for electron collisions with the molecules of the gas. Therefore it is desirable to have a reliable database with cross section benchmarks for these molecules [3–5].

The literature on electron collisions with SiF_4 and GeF_4 (both belonging to the T_d point group) relies on few theoretical and experimental studies. Tossel and Davenport [6] reported elastic cross sections for electron collisions with SiF_4 computed using the multiple scattering-$X\alpha$ method. They found a broad structure located at about 3 eV in the cross section of the T_2 symmetry and a minimum in the cross section of the A_1 symmetry. The negative-ion states of SiF_4 were investigated by Wan *et al.* [7] through the electron transmission (ET) spectroscopy. The authors also measured a total scattering cross section for this molecule for electron impact energies from 0.2 to 12 eV. The derivative of the ET spectra showed a negative-ion state at around 6.5 eV, and the total cross section presented a broad structure at around 8.5 eV. Karwasz *et al.* [8] also obtained experimental total cross sections for electron collisions with SiF_4 using the absolute transmission method for energies between 0.6 and 3500 eV. They reported a structure at 8.5 eV that was interpreted as a shape resonance. Based on a comparison with other fluorinated systems, the authors associated this resonance with electron capture in a threefold-degenerated t orbital. They also found an evidence of a Ramsauer-Townsend minimum at around 1 eV. Curik *et al.* [9] calculated elastic integral and differential cross sections for electron scattering by SiF_4 using a single-expansion method with model potentials for the exchange, correlation, and polarization interactions. The elastic cross section obtained within this approximation showed the presence of a Ramsauer-Townsend minimum at around 0.2 eV and of a shape resonance in the T_2 symmetry located at about 7.2 eV. The shape resonance assignment presented by Curik *et al.* was in agreement with the discussion presented by Karwasz *et al.* [8]. Regarding the presence of a Ramsauer-Townsend minimum, the results of Curik *et al.* also agree with the experimental observations of Karwasz *et al.*, although the minimum in the computed cross section is located below the experiment. More recently, Kato *et al.* [10] measured elastic differential cross sections for SiF_4 for energies from 1.5 eV to 200 eV. They also provided vibrational excitation cross sections that indicated the presence of a shape resonance between 5 eV and 8 eV in the T_2 symmetry. Kato *et al.* also reported cross sections obtained with the independent atom method with the screening-corrected additivity rule (IAM-SCAR). In particular, the authors found good agreement between their measurements and the differential cross sections obtained with the IAM-SCAR method at energies above 10 eV. Bjarnason *et al.* [11] investigated the negative-ion formation in SiF_4 through dissociative electron attachment (DEA). The authors found products of F^-, SiF_3^- and F_2^-, the first two being more intense than F_2^- in the DEA ion yield curves. The authors attributed the F^- and SiF_3^- peaks, located at around 11 eV, to core excited shape resonances in the T_1 (the highest intensity) and T_2 (the higher energy contribution) symmetries. The low-intensity contribution was assigned to a shape resonance in the A_1 symmetry. Electron transport and swarm parameters for SiF_4 were measured by Hunter *et al.* [12]. The authors suggested that the behavior of the electron drift velocity, that presented a negative differential conductivity (which occurs when the electron drift velocity decreases as the electron field $\mathcal{E}$ increases), as a function of the density-reduced electric field $\mathcal{E}/\mathcal{N}$ (where $\mathcal{E}$ is the electron field and $\mathcal{N}$ is the neutral number density), was consistent with the presence of a Ramsauer-Townsend minimum in the cross section and with a large vibrational cross section for this molecule.

The literature on electron scattering with GeF_4 also includes experimental and theoretical works, but in less number than for SiF_4. Szmytkowski *et al.* [13] measured an absolute total cross section for electron collisions with GeF_4 for energies from 0.5 to 250 eV. They reported a peak with maximum located at 6.5 eV and two other peaks at energies above 15 eV. Another feature that deserved attention by the authors was the sharp increase in the total cross section at very low energies. The

authors emphasized that this behavior is typical for electron collisions with polar molecules and was also observed for some nonpolar molecules; for the latter this feature (which in this case the authors referred to as an "anomaly") was discussed in terms of an indirect (resonant) process, such as virtual state and metastable parent negative ion. Kato *et al.* [14] measured differential cross sections for electron impact with GeF_4 for energies from 3 eV to 200 eV. They also computed cross sections with the IAM-SCAR method, and found in general good agrement between the experiment and theory at high energies. A recent calculation on elastic, inelastic, and total cross sections for GeF_4 was carried out by Goswami *et al.* [15]. The authors employed the *ab initio* R-matrix method for energies up to 15 eV and the spherical complex optical theorem (SCOP) model from 15 eV to 5000 eV. In the elastic cross sections the authors reported a shape resonance at 5.69 eV (although the peak is centered at around 7 eV) and assigned it to the T_1 symmetry of T_d, though they have not discussed the sharp increase observed by the experiments of Szmytkowski *et al.* [13]. They calculated differential cross sections and compared their results with the experimental and theoretical results of Kato *et al.* [14], where the agreement improved at 7 eV and 10 eV. Bjarnason *et al.* [11] also investigated the negative-ion formation in GeF_4. They reported several peaks corresponding to the formation of F^-, F_2^-, GeF^-, $GeF_2{}^-$, $GeF_3{}^-$, and $GeF_4{}^-$. In particular, they found peaks for F^- and $GeF_4{}^-$ close to zero energy, which they attributed to a shape resonance in the A_1 symmetry of T_d. The authors associated the ion yield at around 7 eV to a T_2 shape resonance.

Here we present elastic integral, differential, and momentum transfer cross sections for scattering of electrons by SiF_4 and GeF_4. We computed the cross sections using the Schwinger multichannel method with pseudopotentials for energies up to 15 eV. We compare our results with the experimental and theoretical results available in the literature. In particular, we discuss the presence of a Ramsauer-Townsend minimum and of a T_2 shape resonance in the cross sections of SiF_4, and the presence of a virtual state and of a shape resonance in the T_2 symmetry in the cross sections of GeF_4. With these results we aim to help in benchmarking the elastic cross sections for these two molecular targets.

The remainder of this paper is as follows. In Sec. II we describe the theoretical formulation and the computational procedures used in our calculations. In Sec. III we present our results and discussion, and in Sec. IV we close the paper with a summary of our results along with our conclusions.

II. THEORY

The Schwinger Multichannel (SMC) method [16] and its implementation with pseudopotentials (SMCPP) [17] have been recently revised [18], and here we briefly describe those aspects which are important to the present calculations. The SMC method is a variational approach to the scattering amplitude which leads to the following working expression:

$$f^{\mathrm{SMC}}(\vec{k}_f,\vec{k}_i) = -\frac{1}{2\pi}\sum_{m,n}\left\langle S_{\vec{k}_f}\middle|V\middle|\chi_m\right\rangle (d^{-1})_{mn}\left\langle\chi_n\middle|V\middle|S_{\vec{k}_i}\right\rangle, \tag{1}$$

TABLE I. Exponents of the uncontracted Cartesian Gaussian functions used to represent the single-particle basis for Si, Ge, and F atoms.

Type	Si	Ge	F
s	6.143 172	2.429 279	12.545 58
s	3.207 261	1.000 450	6.272 790
s	1.723 970	0.542 241	1.576 479
s	0.176 634	0.148 198	0.499 283
s	0.037 088	0.019 957	0.150 680
s	–	0.005 212	0.077 101
p	3.468 604	1.677 720	9.852 550
p	0.302 834	0.270 291	2.330 403
p	0.091 281	0.091 598	0.462 593
p	0.026 183	0.034 666	0.154 197
p	–	0.011 682	0.051 399
d	0.499 124	0.133 483	0.790 820
d	–	–	0.181 887

where

$$d_{mn} = \langle\chi_m|A^{(+)}|\chi_n\rangle \tag{2}$$

and

$$A^{(+)} = \frac{1}{2}(PV + VP) - VG_P^{(+)}V + \frac{\hat{H}}{N+1} - \frac{1}{2}(\hat{H}P + P\hat{H})\,. \tag{3}$$

In the expressions above, $\{|\chi_m\rangle\}$ represents the $(N+1)$-electron trial configuration-state functions (CSFs), which are products of target states with single-particle scattering orbitals with the proper spin coupling. $|S_{\vec{k}_{i(f)}}\rangle$ is an eigenstate of the unperturbed Hamiltonian H_0, given by the product of a target state and a plane wave with momentum $\vec{k}_{i(f)}$; V is the interaction potential between the incident electron and the target; $\hat{H} \equiv E - H$, where E is the collision energy and $H = H_0 + V$ is the scattering Hamiltonian; P is a projection operator onto the open-channel target space defined as

$$P = \sum_{l=1}^{\text{open}} |\Phi_l\rangle\langle\Phi_l|, \tag{4}$$

and $G_P^{(+)}$ is the free-particle Green's function projected on the P space.

We considered the static-exchange (SE) and the static-exchange plus polarization (SEP) approximations in our calculations. In the SE approximation, the $(N+1)$-electron

TABLE II. Relation between the symmetries of the C_{2v} and T_d groups.

C_{2v}	T_d
A_1	$A_1 + T_2 + E$
A_2	$A_2 + T_1 + E$
B_1	$T_1 + T_2$
B_2	$T_1 + T_2$

TABLE III. Relation between the symmetries of the T_d and C_{2v} groups.

T_d	C_{2v}
A_1	A_1
A_2	A_2
E	$A_1 + A_2$
T_1	$B_1 + B_2 + A_2$
T_2	$A_1 + B_1 + B_2$

basis set is constructed as

$$|\chi_m\rangle = \mathcal{A}|\Phi_1\rangle \otimes |\varphi_m\rangle, \quad (5)$$

where $|\Phi_1\rangle$ is the Hartree-Fock target ground state, $|\varphi_m\rangle$ is a single-particle function, and $\mathcal{A}$ is the antisymmetrization operator. In the SEP approximation, the SE set is augmented by including CSFs constructed as

$$|\chi_{mn}\rangle = \mathcal{A}|\Phi_m\rangle \otimes |\varphi_n\rangle, \quad (6)$$

where $|\Phi_m\rangle$ are N-electron Slater determinants obtained by performing single (virtual) excitations of the target. In the present calculations we considered excitations from the occupied (hole) orbitals to a set of unoccupied (particle) orbitals. $|\varphi_n\rangle$ is also a one-electron function.

We optimized the ground-state geometry (the bond lengths between the Si/Ge atom and the fluorines) of the target at the level of second order Møller-Plesset perturbation theory with the 6-31G(d) basis using the package GAMESS [19], in the T_d group. We employed the local-density *norm-conserving* pseudopotentials of Bachelet *et al.* [20] to represent the nuclei and the core electrons of Si, Ge, and F atoms. The Cartesian Gaussian (single-particle) basis used for Si included $5s4p1d$

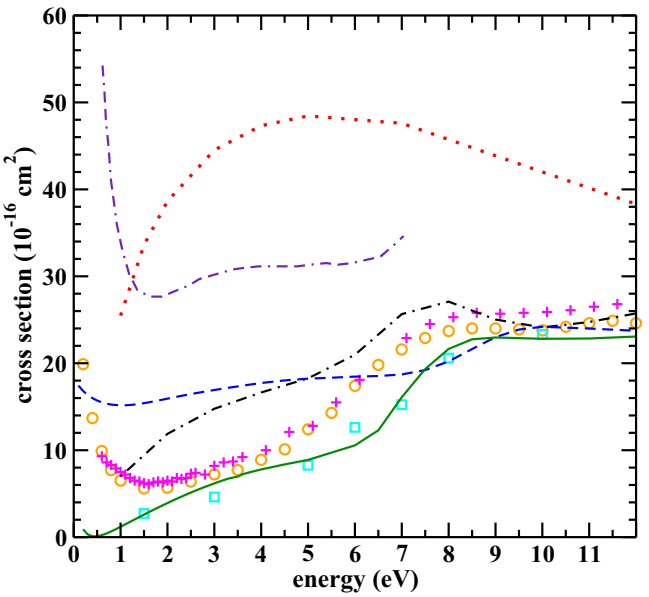

FIG. 1. Integral cross sections for elastic scattering of electrons by SiF_4. Dashed (blue) line, present SE results; solid (dark green) line, present SEP results; dot-dash-dashed (indigo) line, MS-Xα results from Ref. [6]; dot-dashed (black) line, single-center expansion method results of Ref. [9]; dotted (red) line, IAM-SCAR results from Ref. [10]; open (yellow) circles, total cross section of Ref. [7]; crosses (magenta), total cross section of Ref. [8]; squares (cyan), elastic integral cross section (obtained by the integration of the differential cross sections) of Ref. [10].

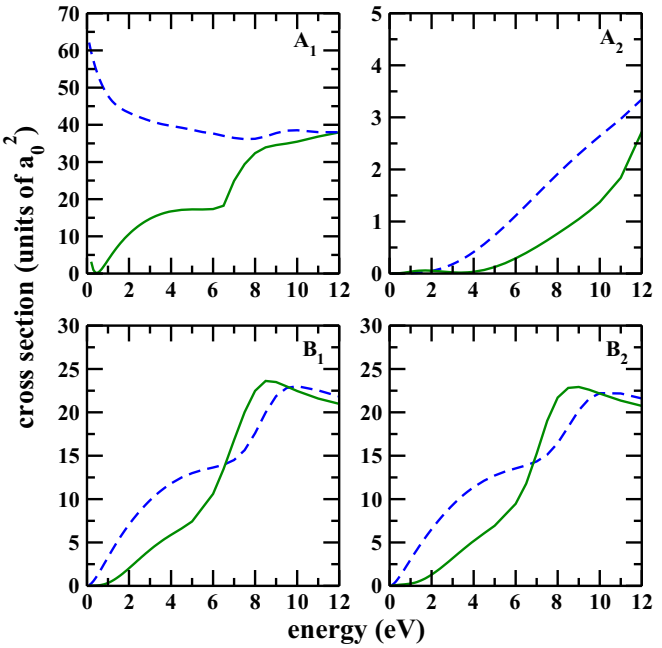

FIG. 2. Symmetry decomposition of the integral cross sections for elastic scattering of electrons by SiF_4 in the C_{2v} group. Solid (dark green) line, present SEP results; dashed (blue) line, present SE results. Cross sections are in units of a_0^2, where a_0 is the Bohr radius and $1a_0 = 0.529\,18 \times 10^{-10}$ m.

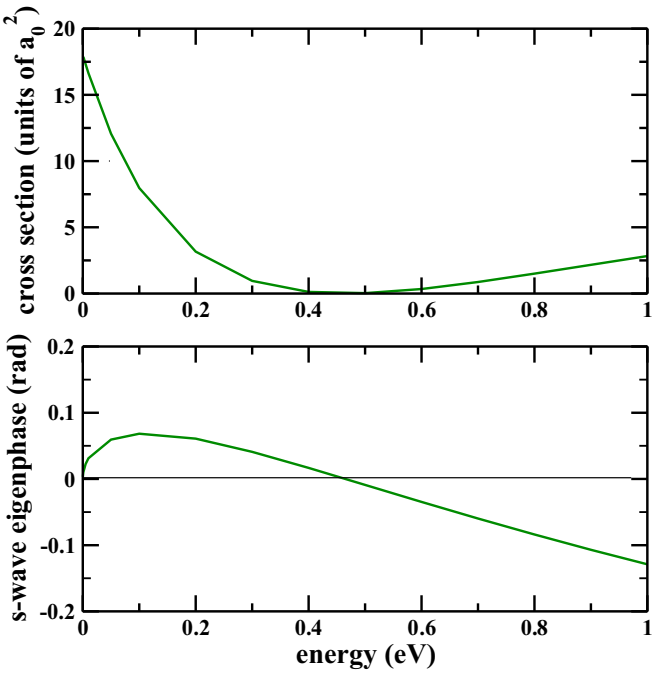

FIG. 3. s-wave cross sections (upper panel) obtained in the SEP approximation and the corresponding s-wave eigenphase (lower panel). See text for discussion.

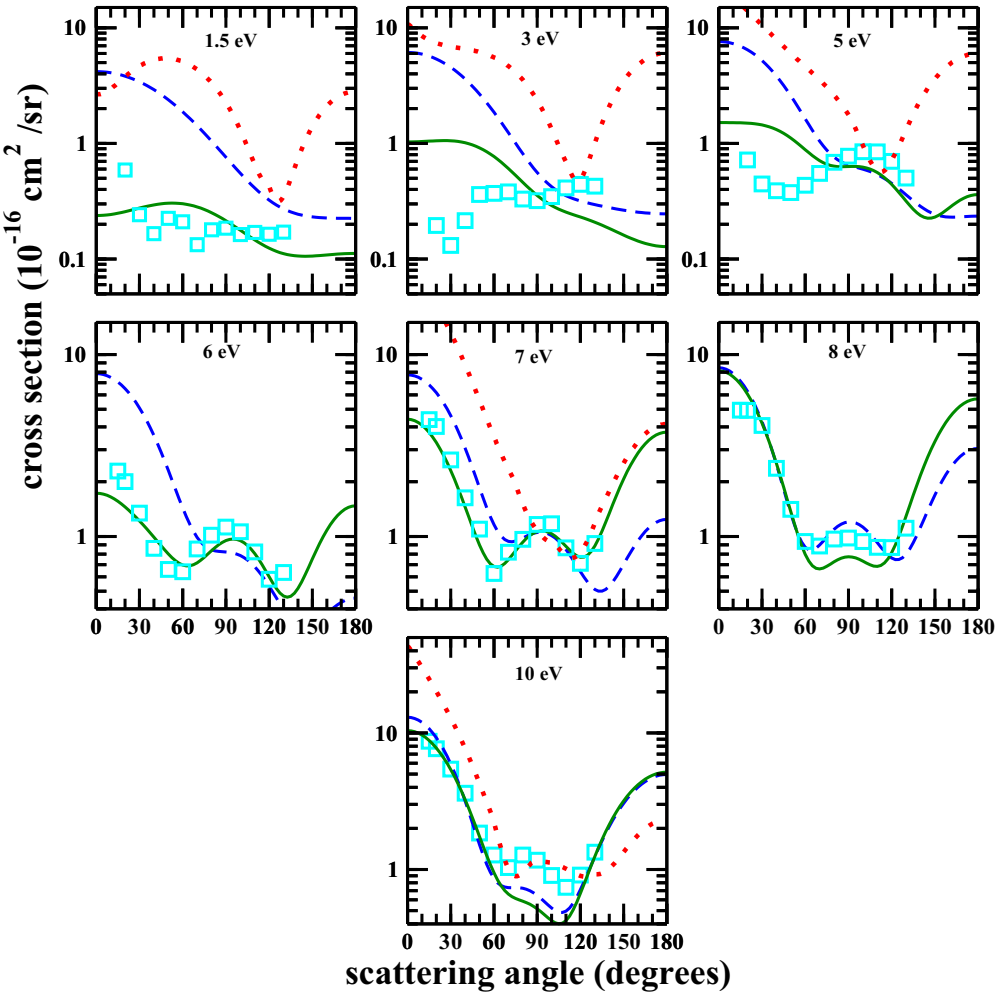

FIG. 4. Differential cross sections for elastic scattering of electrons by SiF_4 at 1.5 eV, 3 eV, 5 eV, 6 eV, 7 eV, 8 eV, and 10 eV. Dashed (blue) line, present SE results; solid (dark green) line, present SEP results; dotted (red) line, IAM-SCAR results from Ref. [10]; squares (cyan); experimental data from Ref. [10].

functions, $6s5p1d$ functions for Ge, and $6s5p2d$ functions for F, which are tabulated in Table I and were generated according to a variation approximation described according to [21].

Since the SMC method deals with Abelian groups, our calculations were carried out within the C_{2v} group and whenever possible the results were discussed in terms of the C_{2v} and T_d groups. The correlations between these two point groups are shown in Tables II and III.

We used improved virtual orbitals (IVOs) [22] to represent the particle and scattering orbitals in the SEP calculations [see Eq. (6)]. For SiF_4 we considered the lowest 49 IVOs, giving 10 108 CSFs for A_1, 9638 for B_1 and B_2, and 9171 for A_2. We used the lowest 52 IVOs for GeF_4, resulting in 11 160 CSFs for A_1, 10 851 for B_1 and B_2, and 10 545 for A_2.

III. RESULTS AND DISCUSSION

A. SIF_4

Figure 1 shows our calculated integral cross section (ICS) in the SE and SEP approximations. In both curves there is a broad structure which is located at around 10 eV in the SE ICS, while in the SEP ICS it is located at around 8.5 eV. There is another feature shown by the SEP ICS that is the deep minimum at around 0.45 eV. In this figure we also show the calculated elastic ICS of Tossel and Davenport [6], the experimental total cross section (TCS) obtained by Wan *et al.* [7] and by Karwasz *et al.* [8], the calculated ICS of Curik *et al.* [9], and the elastic ICSs obtained with the IAM-SCAR method and by the integration of the measured differential cross sections (after their extrapolation to 0° and 180°) of Kato *et al.* [10]. All cross sections show a broad structure at around 8 eV, except for the ICS of Tossel and Davenport [6], where this feature is located at 3 eV, and for the IAM-SCAR ICS (that provides better results at energies above 20 eV). The TCSs of Wan *et al.* [7] and Karwasz *et al.* [8] show a minimum at around 1.5 eV. In general, our results agree well in shape with the other cross sections and show good agreement with the integrated ICS of Kato *et al.* [10].

In Fig. 2 we present the symmetry decomposition of the integral cross section according to the C_{2v} point group obtained in both SE and SEP approximations. The minimum seen in the SEP ICS of Fig. 1 is from the A_1 symmetry, and the broad structure has contributions from the A_1, B_1, and B_2 symmetries and corresponds to the shape resonance in

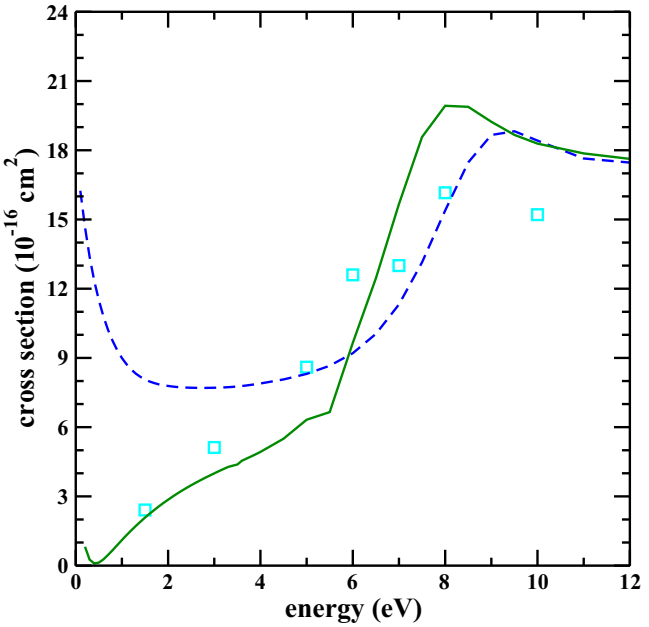

FIG. 5. Momentum transfer cross section for elastic scattering of electrons with SiF_4. Dashed (blue) line, present SE results; solid (dark green) line, present SEP results; squares (cyan), experimental data from Ref. [10].

the (threefold-degenerated) T_2 symmetry discussed by the previous works.

In order to investigate the minimum in the SEP ICS of the A_1 symmetry we looked at the s-wave ($\ell = 0$ partial wave) cross section and the corresponding eigenphase for energies up to

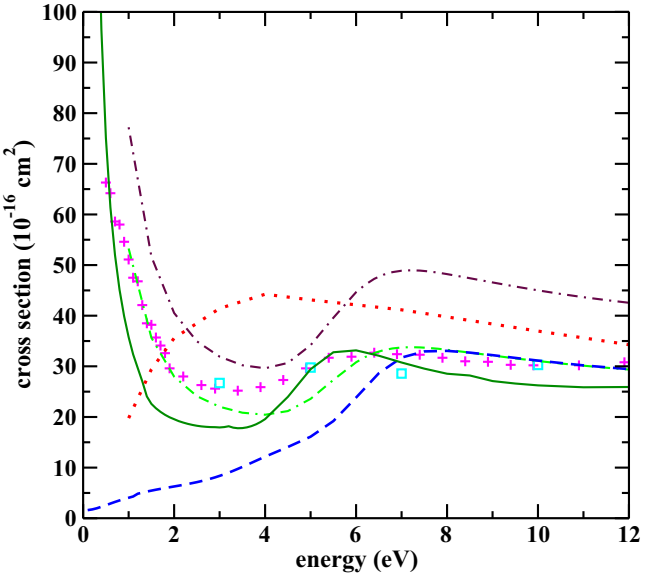

FIG. 6. Integral cross sections for elastic scattering of electrons by GeF_4. Dashed (blue) line, present SE results; solid (dark green) line, present SEP results; dotted (red) line, IAM-SCAR results from Ref. [14]; dot-dashed (brown) line, R-matrix results from Ref. [15]; dot-dash-dashed (green) line, scaled R-matrix results from Ref. [15]; crosses (magenta), total cross section of Ref. [13]; squares (cyan), elastic integral cross section of Ref. [14]. See text for discussion.

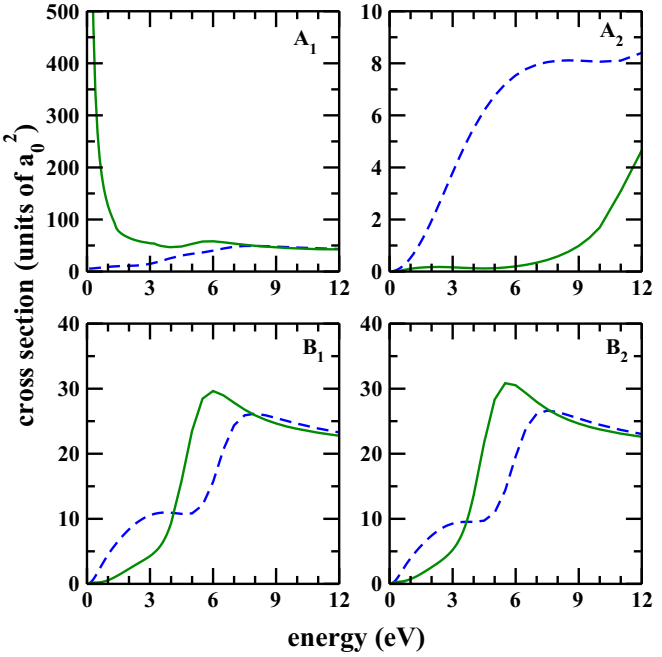

FIG. 7. Symmetry decomposition of the integral cross sections for elastic scattering of electrons by GeF_4 in the C_{2v} group. Solid (dark green) line, present SEP results; dashed (blue) line, present SE results. Cross sections are in units of a_0^2, where a_0 is the Bohr radius and $1a_0 = 0.529\,18 \times 10^{-10}$ m.

1 eV. Figure 3 shows that the minimum is located at 0.45 eV and the eigenphase changes sign, crossing zero at the same energy. Since for an attractive potential the eigenphase is positive and for a repulsive potential it is negative, the sign change in the

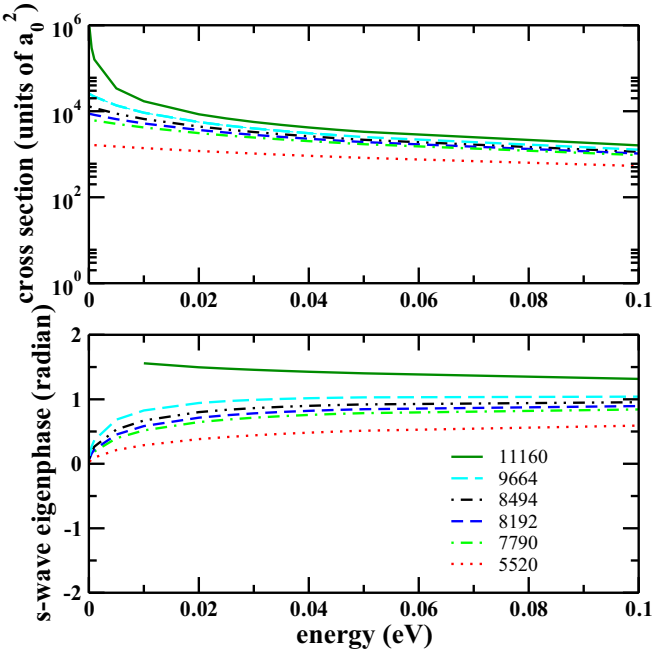

FIG. 8. Present A_1 cross sections (upper panel) and the s-wave eigenphase (lower panel) obtained in the SEP approximation obtained with different number of CSFs in the expansion of the $(N+1)$-electron trial basis set. See text for discussion.

TABLE IV. Number of CSFs (NCSFs) in the $(N+1)$-electron trial basis set and the scattering length α in units of a_0^2, where a_0 is the Bohr radius and $1a_0 = 0.529\,18 \times 10^{-10}$ m. See text for discussion.

NCSFs	α
11160	–
9664	–45,32
8494	–32,18
8192	–26,48
7790	–22,60
5520	–11,48

eigenphase means that the potential changes from attractive to repulsive. In the SEP approximation the net scattering potential is given by the static and polarization potentials, which are attractive, and by the exchange potential, which is repulsive (as required by Pauli's exclusion principle). The Ramsauer-Townsend (RT) minimum is a consequence of the cancellation between the attractive and repulsive potentials [23,24]. Note that this minimum is not present in the SE cross section (no polarization potential). The presence of the RT minimum in the cross section of SiF_4 is also consistent with the observations of Hunter *et al.* [12].

The differential cross sections (DCSs) are shown in Fig. 4 for energies of 1.5 eV, 3 eV, 5 eV, 6 eV, 7 eV, 8 eV, and 10 eV. We show both the SE and SEP results in comparison with the experimental and theoretical results of Kato *et al.* [10]. For energies below 6 eV there is a big discrepancy between our results and the experiment and with the results obtained by the IAM-SCAR method (which is know to give reliable results at higher energies). At 6 eV and for higher energies the agreement between our SEP results and the experiment improves, and the two minima seen in the DCSs correspond to a major contribution from d wave ($\ell = 2$ partial wave). At 10 eV the IAM-SCAR results agree better than ours with the experiment at intermediate scattering angles.

Figure 5 presents the momentum transfer cross section (MTCS) for SiF_4 obtained in the SE and SEP approximations. The results of Kato *et al.* [10] are also shown. These authors integrated the DCSs weighted by the factor $1 - \cos\theta$. In general our results obtained in the SEP approximation agree well with the MTCS of Kato *et al.* [10] for energies below

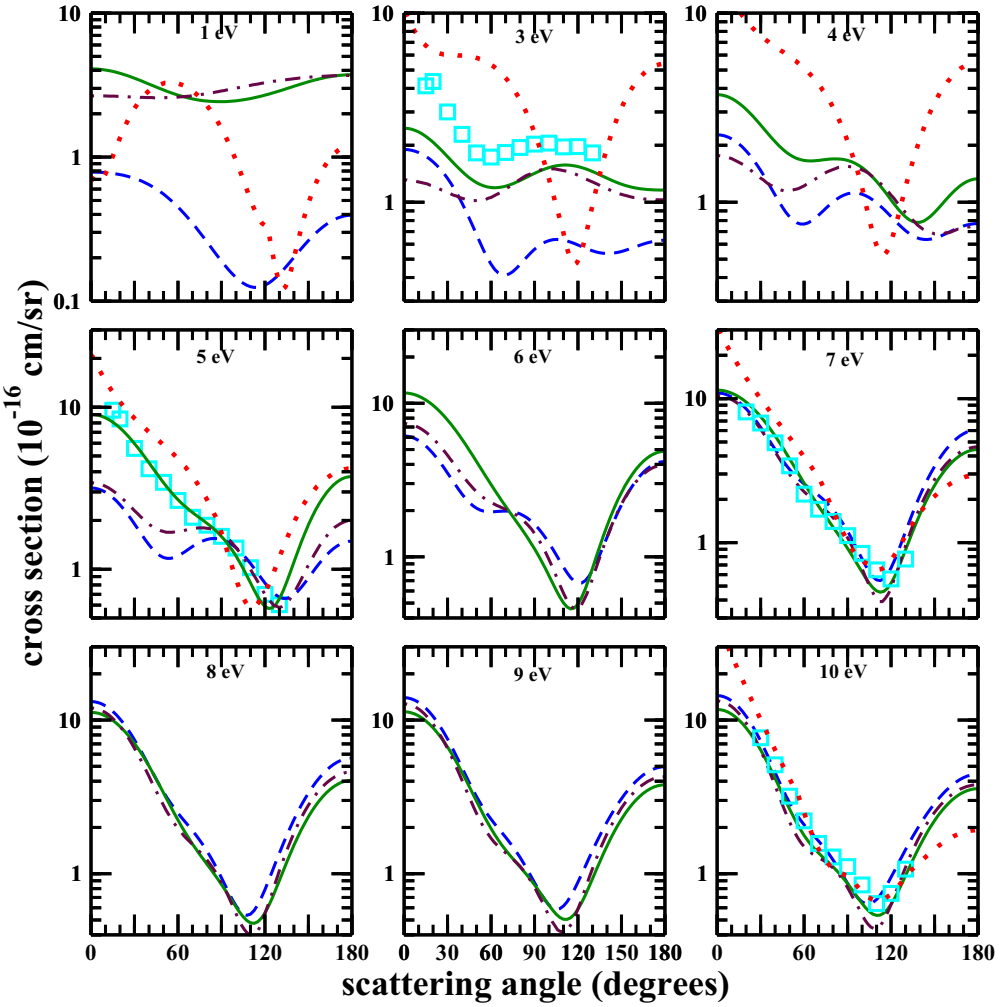

FIG. 9. Differential cross sections for elastic scattering of electrons by GeF_4 at 1 eV, 3 eV, 4 eV, 5 eV, 6 eV, 7 eV, 8 eV, 9 eV, and 10 eV. Dashed (blue) line, present SE results; solid (dark green) line, present SEP results; dotted (red) line, IAM-SCAR results from Ref. [14]; squares (cyan); experimental data from Ref. [14]; dot-dashed (brown) line, R-matrix results from Ref. [15].

8 eV and show qualitative agreement at energies above 8 eV. The RT minimum is also present in the SEP MTCS.

B. GeF_4

Figure 6 shows the present ICS in the SE and SEP approximations. There are two main features shown by the SEP ICS: the sharp increase at lower energies and the broad structure located at around 6 eV, which is also seen in the SE ICS centered at around 8 eV. We show for comparison the TCS of Szmytkowski *et al.* [13], the elastic ICSs of Kato *et al.* [14] obtained by the integration of the measured DCSs and also computed with the IAM-SCAR method, and the calculated ICS by Goswami *et al.* [15] obtained with the *R*-matrix method. The TCS of Szmytkowski *et al.* [13] and the ICS of Goswami *et al.* [15] also show the two features mentioned above, where the broad structure (assigned to the T_1 symmetry) is located at 7 eV. The integrated ICS of Kato *et al.* [14] begins at 3 eV and the broad structure is barely seen in the ICS plot. The results of Goswami *et al.* [15] agree well with ours in shape, but they are overestimated, being larger even than the TCS. We suspect that there is a conversion factor missed in their results, and we normalized the ICS of Goswami *et al.* to our SE ICS at 9 eV. The normalized ICS agrees well with our SE ICS for energies above 8 eV, suggesting that the authors have not included enough polarization to bring the broad shape resonance in agreement with the experimental location. Although Goswami *et al.* [15] also observed the increase of the ICS at lower energies, they have not discussed this feature in their paper. The ICS obtained with the IAM-SCAR method, although higher in magnitude than the experiment and our results, follows the shape of the ICSs and TCSs for energies above 6 eV. As mentioned before, this method works quite well at high energies.

We present in Fig. 7 the symmetry decomposition of the ICS for GeF_4 in the C_{2v} group. The broad structure presented by the ICS has contributions from the A_1, B_1, and B_2 symmetries, and corresponds to the T_2 symmetry of T_d, which is threefold degenerate. The increase at low energies is seen in the component of the ICS belonging to the A_1 symmetry. Szmytkowski *et al.* [13] discussed this feature, which is characteristic of polar molecules and was also observed in some nonpolar molecules, as a resonance at zero energy. In order to interpret this behavior, we computed the A_1 cross section and the *s*-wave eigenphase with different numbers of CSFs, and the results are shown in Fig. 8. We note that the eigenphase shows a more dramatic increase from 0 radians towards $\pi/2$ radians as the number of CSFs is augmented, followed by the increase in magnitude of the corresponding cross sections, especially close to zero energy. We also computed the scattering length using the approximation suggested by Morrison [25] and found negative values in all cases, as shown in Table IV. In particular, the eigenphase computed with 11 160 CSFs in the $(N+1)$-electron trial basis set presented an unstable behavior at very low energies and therefore it was not possible to compute the scattering length for this calculation. However, by the extrapolation of the *s*-wave eigenphase shown in Fig. 8 corresponding to this larger calculation, it is possible to argue that it tends to a value close to $\pi/2$ as the energy tends to zero. Using Lagrange and Newton polynomials along with

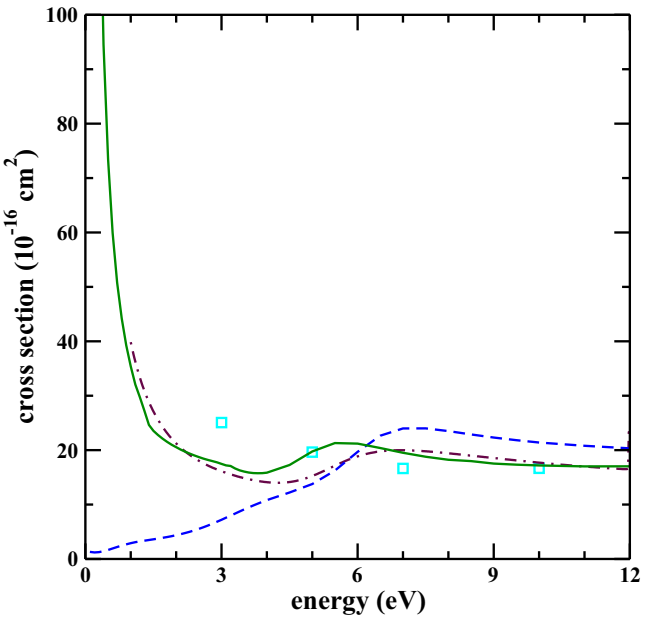

FIG. 10. Momentum transfer cross section for elastic scattering of electrons with GeF_4. Dashed (blue) line, present SE results; solid (dark green) line, present SEP results; squares (cyan), experimental data from Ref. [14]; dot-dashed (brown) line, *R*-matrix results from Ref. [15].

18 eigenphase values from 0.01 eV up to 1 eV to compute the eigenphase at zero energy, we obtained the values of 1.71 radians and 1.54 radians, respectively, which are close to $\pi/2$. The cross section obtained with 11 160 CFSs shows a bigger increase than in the other cases. The behavior of the *s*-wave eigenphase and the A_1 cross sections, along with the negative values of the computed scattering lengths suggest the presence of a virtual state in the GeF_4 cross section, as suspected by Szmytkowski *et al.* [13].

Bjarnason *et al.* [11] investigated the negative-ion formation in GeF_4 and found peaks at zero energy corresponding to the formation of F^- and GeF_4^-. The authors attributed these peaks to a shape resonance in the A_1 symmetry close to zero energy. Our results show that the formation of these anions are related to the virtual state observed by the measurements of Szmytkowski *et al.* [13] and by our calculations. Bjarnason *et al.* [11] also found peaks corresponding to the formation of F^- at 7 eV, which were attributed to a shape resonance in the T_2 symmetry. This interpretation is consistent with the results presented by Szmytkowski *et al.* [13] and by our calculations.

The DCSs for GeF_4 are shown in Fig. 9. We present our SE and SEP DCSs, the experimental data and IAM-SCAR results of Kato *et al.* [14] and the *R*-matrix DCSs of Goswami *et al.* [15]. Our SEP DCSs agree well with the experiment at 3 eV, mostly in shape, and at 5 and 7 eV in shape and magnitude. Our SEP results also agree well with the *R*-matrix results at 7 eV and energies higher than that. At 4 eV, 5 eV, and 6 eV, the DCSs of Goswami *et al.* [15] agree better with our SE DCSs than with our DCSs computed in the SEP approximation, suggesting that they did not account properly for polarization in their calculations. In particular, our SEP

results agree well with the IAM-SCAR DCSs at 5 eV, 7 eV, and 10 eV.

Our calculated MTCSs are shown in Fig. 10, along with the results of Kato *et al.* [14] and the *R*-matrix results of Goswami *et al.* [15]. The two calculations agree well with each other in shape and also with the experiment. The main difference between the two calculations is the location of the shape resonance, where in the *R*-matrix MTCS the peak is located at an energy higher than ours.

IV. SUMMARY

We presented elastic integral, differential, and momentum transfer cross sections for electron scattering by the tetrahalides molecules SiF_4 and GeF_4. In general, our results for both molecules showed good agreement with the available experimental data and with the results from calculations using different methods. The integral cross section of SiF_4 obtained in the static-exchange plus polarization approximation showed the presence of a shape resonance in the T_2 symmetry centered at about 8.5 eV, and of a Ramsauer-Townsend minimum located at 0.45 eV. These two features have also been observed by other groups. Our differential cross sections showed good agreement with the experimental data for energies above 5 eV. We found the presence of a T_2 shape resonance located at about 6 eV and of a virtual state in the cross section of GeF_4 obtained in the static-exchange plus polarization approximation. Both results were also reported by previous calculations and experiments. The present differential cross sections showed good agreement with the results of other calculations and with experiment for energies of 5 eV, 7 eV, and 10 eV.

ACKNOWLEDGMENTS

G.M.M. acknowledges support from the Brazilian Agency Coordenação de Aperfeiçoamento de Pessoal de Nível Superior (CAPES). M.H.F.B. acknowledges support from the Brazilian Agency Conselho Nacional de Desenvolvimento Científico e Tecnológico (CNPq) and from Financiadora de Estudos e Projetos (Finep) (under project CT-Infra). M.H.F.B. also acknowledges computational support from CENAPAD-SP. The authors acknowledge Prof. Carlos de Carvalho for computational support at LFTC-DFis-UFPR and LCPAD-UFPR.

[1] M. A. Lieberman and A. J. Lichtenberg, *Principles of Plasma Discharges and Materials Processing* (John Wiley & Sons, New York, 1994).
[2] W. N. G. Hitchon, *Plasma Processes for Semiconductor Fabrication* (Cambridge University Press, Cambridge, UK, 1999).
[3] L. G. Christophorou and J. K. Olthoff, J. Phys. Chem. Ref. Data **28**, 967 (1999).
[4] L. G. Christophorou and J. K. Olthoff, Appl. Surf. Sci. **192**, 309 (2002).
[5] J.-S. Yoon, M.-Y. Song, H. Kato, M. Hoshino, H. Tanaka, M. J. Brunger, S. J. Buckman, and H. Cho, J. Phys. Chem. Ref. Data **39**, 033106 (2010).
[6] J. A. Tossel and J. W. Davenport, J. Chem. Phys. **80**, 813 (1984); **83**, 4824 (1985).
[7] H-X. Wan, J. H. Moore, and J. A. Tossel, J. Chem. Phys. **91**, 7340 (1989).
[8] G. P. Karwasz, R. S. Brusa, A. Piazza, A. Zecca, P. Mozejko, G. Kasperski, and C. Szmytkowski, Chem. Phys. Lett. **284**, 128 (1998).
[9] R. Curik, F. A. Gianturco, and N. Sanna, Int. J. Quantum Chem. **84**, 565 (2001).
[10] H. Kato, K. Anzai, T. Ishihara, M. Hoshino, F. Blanco, G. García, P. Limão-Vieira, M. J. Brunger, S. J. Buckman, and H. Tanaka, J. Phys. B: At., Mol. Opt. Phys. **45**, 095204 (2012).
[11] E. H. Bjarnason, F. H. Ómarsson, M. Hoshino, H. Tanaka, M. J. Brunger, P. Limão-Vieira, and O. Ingólfsson, Int. J. Mass Spectrom. **339-340**, 45 (2013).
[12] S. R. Hunter, J. G. Carter, and L. G. Christophorou, J. Appl. Phys. **65**, 1858 (1989).
[13] C. Szmytkowski, P. Mozejko, and G. Kasperski, J. Phys. B: At., Mol. Opt. Phys. **31**, 3917 (1998).
[14] H. Kato, A. Suga, M. Hoshino, F. Blanco, G. García, P. Limão-Vieira, M. J. Brunger, and H. Tanaka, J. Chem. Phys. **136**, 134313 (2012).
[15] B. Goswami, R. Naghma, and B. Antony, RSC Adv. **4**, 63817 (2014).
[16] K. Takatsuka and V. McKoy, Phys. Rev. A **24**, 2473 (1981); **30**, 1734 (1984).
[17] M. H. F. Bettega, L. G. Ferreira, and M. A. P. Lima, Phys. Rev. A **47**, 1111 (1993).
[18] R. F. da Costa, M. T. do N. Varella, M. H. F. Bettega, and M. A. P. Lima, Eur. Phys. J. D **69**, 159 (2015).
[19] M. W. Schmidt, K. K. Baldridge, J. A. Boatz, S. T. Elbert, M. S. Gordon, J. H. Jensen, S. Koseki, N. Matsunaga, K. A. Nguyen, S. J. Su, T. L. Windus, M. Dupuis, and J. A. Montgomery, J. Comput. Chem. **14**, 1347 (1993).
[20] G. B. Bachelet, D. R. Hamann, and M. Schlüter, Phys. Rev. B **26**, 4199 (1982).
[21] M. H. F. Bettega, A. P. P. Natalense, M. A. P. Lima, and L. G. Ferreira, Int. J. Quantum Chem. **60**, 821 (1996).
[22] W. J. Hunt, and W. A. Goddard III, Chem. Phys. Lett. **3**, 414 (1969).
[23] M. A. P. Lima, K. Watari, and V. McKoy, Phys. Rev. A **39**, 4312 (1989).
[24] B. M. Nestmann, K. Pfingst, and S. D. Peyerimhoff, J. Phys. B: At., Mol. Opt. Phys. **27**, 2297 (1994).
[25] M. A. Morrison, Phys. Rev. A **25**, 1445 (1982).